9C-2D Seismic data analysis: Olds, Alberta

Grace Y.C. Yang and Robert R. Stewart

ABSTRACT

This paper discusses procedures to interpret nine-component, 2-D seismic data. These procedures are used to differentiate productive dolomite from non-productive limestone and estimate the trends of permeability.

P-wave and *S*-wave vibrators were used in this study over a 10.3 km line. Three-component receivers recorded each source orientation. The *P-P* wave data are excellent, the *P-SV* data is very good. *SH-SH* data are somewhat nosier. The other sections are marginal.

The analysis technique employed measures the traveltime, the amplitudes and the velocity ratio of the shear (*S*) and compressional (*P*)-wave directly from stacked seismic sections. At each surface position along this seismic line, the ratio of the shear to compressional traveltime and Poisson's ratio near the target horizon are calculated and plotted as a function of shot points. There is a strong correlation between the observed lateral variation in the measured *S* and *P* wave travel time, their ratio, and Poisson's ratio with known facies changes in the geological cross section.

This study indicates that it is possible to separate the low permeability bedded facies from the high permeability stramotoporoid using the analysis of traveltime of a given interval among the various component seismic data. The plots of the *P*- and *S*- wave velocity, such as V_p/V_S ,V_S/V_{SV} or V_S/V_{SH} versus shot points show that this seismic line can be separated into three different regions of various V_p/V_S values: The average V_p/V_S value of 1.73 on the east and average value of 1.65 on the west coincide with the higher permeability facies whereas the low average value of 1.50 in the middle corresponds to the low permeability bedded facies. The plots of Poisson's ratio also show similar separations. These results refines the geological model (base on cores) and improve our knowledge of the distribution of permeability and porosity trend in the area.

INTRODUCTION

The application of shear (*S*)-wave seismic data in petroleum exploration has received increasing attention in recent years. The use of *S*-wave technology has led to the multicomponent survey which has proven effective in analyzing lithology changes. However, high acquisition and processing costs have limited the availability of nine-component seismic data.

In 1993, Amerada Hess Corporation Limited (AHCL), conducted a shear-wave program in Olds, 65 km north of Calgary, Alberta (Figure 1). An elastic-wave nine-component seismic line was acquired across a 145 km long productive trend in the Devonian Wabamun Crossfield member. The survey's primary purpose was to determine if *S*-wave data could define high porosity and permeable trends within the reservoir. The seismic line, 10.3 km long, runs east - west in Twp. 32, Rge. 1 and Rge. 2 W5 (Figure 2).

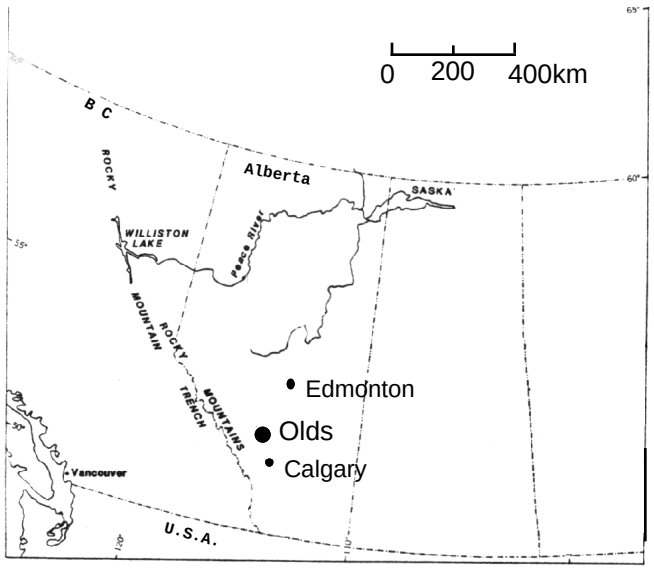

Fig. 1. Location of the study area

This multicomponent survey consists of three vibratory sources (*P*-wave source - in vertical (z) direction, *SV* wave source - in horizontal (x) direction, *SH* wave source - in horizontal (y) direction) and three orthogonal receivers (vertical, radial and transverse) which yield nine unique observations. These nine components are illustrated in Table 1 as a function of source receiver polarization.

The availability of Olds data set provides an excellent opportunity for a combined interpretation of the *P* -, the *S* -, and converted waves, also for evaluating the power of *S*-wave survey and its effect in providing additional information about rock type, porosity and pore fluid content. We will use *P-P*, *P-SV*, *SH-SH*, *P-SH*, and *SV-SV* for more detailed analysis in this study. However, since some clear signals are observed on the shear converted data, such as *SH-SV*, *SH-P*, *SV-SH*, and *SV-P* data set, anisotropy analysis is also discussed.

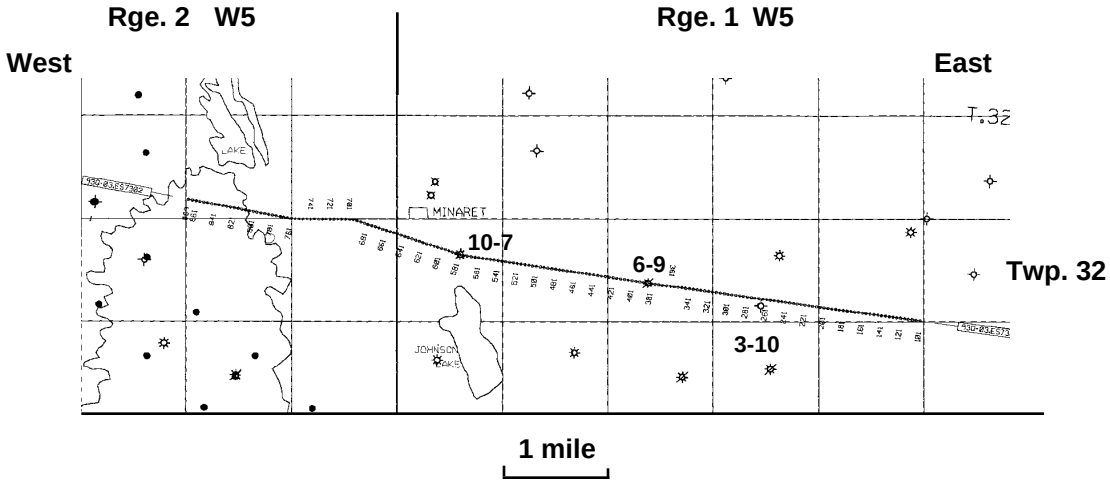

Fig. 2 Location of seismic line

	vertical	radial	transverse
receivers / sources	*P* (z)	*SV* (x)	*SH* (y)
P (Z)	*P-P*	*P-SV*	*P-SH*
SV (X)	*SV-P*	*SV-SV*	*SV-SH*
SH (Y)	*SH-P*	*SH-SV*	*SH-SH*

Table 1. Multicomponent survey

GEOLOGICAL BACKGROUND

In the Olds gas field, production is obtained from a dolomitized porous zone in the Devonian carbonate section. The zone of interest is the Crossfield member within the carbonate section. During middle Wabamun time, a period of more open marine conditions (and / or transgression) resulted in the deposition of a north-south trending belt of calcarenitic and bioclastic banks in the Okotoks-Calgary-Olds area. These banks together with associated tidal flat and shallow shelf deposits form the Crossfield Member dolomites which are encased in anhydrite. The proposed depositional model is shown in Figure 3 (AHCL, 1993). North - south trending open marine bedded facies (high permeability) were on the west, Sabkha anhydrite facies and bedded mottled facies (low permeability) were at east. Tabular stromotoporoids, or irregular stramotoporoids fragments developed on the shoal. A local facies change exists as the result of a stramotoporoid and algal bank development at the time of deposition. The stratigraphic nomenclature and distribution facies are illustrated in Figure 4 (AHCL, 1993).

Porosity is found in dolomitized rocks, originally organic pore space. Porosity development varies with the considerable variations in lithology, and is further complicated by anhydrite and calcite cement filling some of the original pore space. The net pay is about 5 to 11 meters thick with porosity ranges from 6 to 7 %. It has a proven reserves of 125 Bcf, plus associated liquid and sulfur volumes. The H_2S production is 5 to 33%.

In the Olds gas field, the permeability ranges from 3 to 500 md (commonly < 100 md). 10-7-32-1W5 has a permeability of 100 md. Porosity and fluid saturation distribution control the hydrocarbon reserves in place, while permeability is the key parameter determining rate of production. The nature of the porosity in carbonates can be ascertained only from cores. Wire line logs can give information on the total amount of porosity, but little or nothing on its nature. Frequently, permeability increases with porosity. The geological attributes of reservoir quality can be stated as follows:

1. Depositional environment and diagenetic history control the distribution of porosity and permeability in lateral and vertical directions giving rise to reservoir heterogeneity.

2. Permeability distribution in a reservoir rock is dictated by bedding type (mega-scopic) and the textural variations (micro-scopic) in each bed.

3. Fractures create preferential flow paths and bioturbation destroys permeability. If the porosity is low, and the permeability is high, that could be an indication of the existence of fractures. Permeability of fractures is a direct function of the fracture width (Fertl, 1978):

$$k \text{ (darcy)} = 8.43 \times 10^6 \times w^2 \qquad (1)$$

$$w = \text{fracture width, (cm).}$$

A fracture with a tiny width of 0.001 cm will have a permeability of 8.43 darcys. It is hoped that *S*-wave data could define high porosity and permeability trend within the reservoir.

DATA SET

The 10.3 km and 4500 m spread nine-component line, starting at shot point 101 in the east to shot point 869 at west end, as shown in Figure 2, crosses a north-south 145 km long productive trend (Figure 3) in the Devonian Wabamun Crossfield member. Three wells have been drilled at the indicated locations along the line: 10-7-32-1W5, within 153 m from the line near shot point 581; 6-9-32-1 W5, within 113 m from the line near shot point 381; and 3-10-32-1W5 at shot point 265. Well 10-7-32-1 W5 has produced 54 Bcf of gas with porosity of 6% and permeability of 100 md Well 6-9-32-1 W5 encountered tight dolomites, and 3-10-32-1W5 is wet.

This nine-component seismic data were acquired using a conventional P-wave vibrator, a *SV*-wave and a *SH*-wave vibrators. The source vibrated at every station (VP) and each VP has 2 sweeps with a sweep from 8 to 80 Hz for P-wave and 8 to 50 Hz for S-wave. The recording has a 2 ms sample interval. A fixed receiver spread is used with a total of 300 three-component geophones at 15 m spacing. The source interval was 90 m, and group spacing was 15m. With 300 traces per spread, it yielded 50 fold CDP coverage. The sweep length was 12 seconds through which the vibrators have the ability to control the source waveform and the signal - to - noise ratio of the seismic data. The parameters of the survey are detailed in Table 2.

The data set were processed by Pulsonic Geophysical Ltd. The flow for the *P-P* and *P-S* data are given in the Table 3. Table 4 listed the flow of *S* and *S-P* data. The differences among different data sets are highlighted in bold cases. The general quality of the final stacked sections are shown in Figures 5a to 5i.

The general quality of *P*, *P-SV*, and *SH* is good. Some portions of *SV*, *SV-P*, and *P-SH* data have very high S/N ratio. *SH-P* data is pure noise. *SH-SV* and *SV-SH* data are relatively noisy, primary reflections can hardly be identified (Figure 5f-5i). However, some signal is visible on *SV-SH* and *SH-SV* components on the eastern portion of the line. Note that the time scale of S-wave is 3.75 in / sec, and is 5 in /sec for the converted -wave sections. The *P*-wave time scale is 7.5 in /sec as usual.

ANALYSIS AND INTERPRETATION

The interpretation of the multicomponent seismic data hinges upon the correlation between the *P*, the *S*, or the converted waves, so that their velocities and time information can be related to specific formation. We take a straight forward approach to interpret the nine-component seismic data. An offset *P* -wave synthetic seismogram was generated using the sonic log from 10-7-32-1W5.

The Crossfield *P*-wave reflection generally does not discriminate between porous and tight zones. Figure 6 show the seismic characters of *P-P*, *P-SV* and *SH-SH* side by side near wells of 10-7 and 6-9. Reflections from the Wabamun - Banff formations occur at about 1.3 s on the *P-P* data, at about 1.95 s on the *P* -converted (*P-SV* or *P-SH*) data, and at about 2.6 s on shear data. The near two-to-one correlation is apparent, with the most deviation in the shallow portion of the section. The compacted deeper section is generally more homogeneous than the shallower sections. For this reason, the correlation often start in the deeper portion of the section. Figure 7 shows the correlations between the *P*, the *P*-converted, and *SH* components.

Three key horizons (as indicated in figures 5a, 5b and 5c) near the Crossfield reservoir were selected because of their continuity. These horizons are interpreted and mapped from all five component data. The traveltime for each horizon intervals just above the Crossfield member (**l**ow event to **s**trong event, **l**ow event to **t**op event, and **s**trong event to **t**op event) were measured at every 10 shot points from five components sections. The t_s / t_p values exhibit fluctuations along the line of section, so a smoothing function has been applied to show more significant lateral variations.

Ratios of the *P*-wave and S-wave velocity, such as V_p/V_s (where V_s represents velocity of converted *P-SV* wave), or V_s/V_{sv} or V_s/V_{sH} were plotted versus shot points (Figure 8). They show that this seismic line can be separated into three different regions based on the three distinct ratios: east of shot point of 320 with a higher average value of 1.73, west of shot point of 540 with an average ratio of 1.65, and a larger variation in the middle region with an average ratio as low as 1.50. The plots of Poisson's ratio σ (= 1.5 $(V_p/V_s)^2$ - 1] / [$(V_p/V_s)^2$ - 1]) versus shot points also show similar separations (Figures 9).

When tied to well control and the geological facies map (Figure 3), the correlation of the three regions is quite interesting. It indicates that the observed V_p/V_s (or $2*t_{ps} / t_{pp}$ $_{-1}$) values in excess of 1.73 correspond to the tight limestone sequence (east of shot point 320). West of shot point of 540, yields an average $2*t_{ps} / t_{pp}$ $_{-1}$ value of 1.65, predominately dolomites. The middle region (could it be the bedded and mottled facies ?) of V_p/V_s value of 1.5, separates the west region (more porous dolomites / or gas area) with the east region (tight limestone or water bearing zone). The values of these ratios may not represent the threshold values for lithology or pore fluid, but the boundaries of these distinct lateral difference are good indicators of lithology. They will aid in refining the geological facies map.

Figure 10 shows the relationship between the Poisson's ratio and the ratio of travel time of P-component and S-component through a given layer. Plot of $2*V_{sH} /V_s$ $-V_{sH}$ $/V_p$ which is equivalent to interval velocity ratio of V_{sH} /V_{sv} of formations bounded by same events (Figure 11) also shows three distinguished regions. West of shot point 540, the ratio of V_{sH} / V_{sv} is more constant at value of 1.2.

Lateral variations in the ratio of the *SH*-wave velocity to the *SV*-wave velocity could provide an estimate of the degree of *S*-wave anisotropy present within the stratigraphic sequence (Justice, 1984). Seismic anisotropy is the variation in velocity as a function of direction of propagation and may be associated with propagation through fracture zones. Thus inferring stress field or fracture orientation and fracture density may be possible.

Extraction of relevant differences, such as variations in amplitudes of the P- and S-wave reflections between the different data sets also reveal similar lithological separation (not shown here). Both east and west portions of the line show larger amplitude differences compared with the middle portion where very little amplitude difference is observed.

DISCUSSION

This project is to study lateral variations of reservoir quality through analysis of *P*-wave and *S*- wave sections, the V_p/V_s values as well as amplitudes. Once identical reflection horizons are identified on different data components, the time ratio can be determined. In the Olds Gas Field, the reservoir dolomite is encased in anhydrite which has compressional velocities similar to those of dolomite. The shear-wave velocity appears to change however. Through the analysis of Poisson's ratio or, equivalently, by the ratio of *P*- to *S*-wave velocity from multi-component seismic data along the seismic line, we find interesting facies correlation with V_p/V_s.

CONCLUSIONS

1. In terms of the quality of each component: *P-P* and *P-SV* have the best quality, *SH-SH* is superior to *SV-SV*. As of the other converted data sets: *SV-P* is better than *P-SH* and *SH-SV, SV-SH* or *SH-P*.

2. The analysis of the Olds nine-component seismic survey has provided ways to differentiate the changed facies of the reservoir previously unattainable with conventional *P-P* seismic and well data. The geological facies map is further refined base on the *Vp/Vs* ratio. Lower *Vp/Vs* ratio corresponds to tight or low permeability lithology, and higher *Vp/Vs* ratio correspond to more porous or higher permeability lithology. *Vp/Vs* ratio is the most useful measurement for reservoir studies.

3. The comparison of extracted amplitudes between different components also suggested that shear wave data related to lithology more directly than *P* -wave data.

4. The signals viewed on the shear-wave converted data and the velocity ratio of shear wave data analysis all indicated that some anisotropy presence in the area, whether it is any indication of fracture is unknown without further investigation.

FUTURE WORK

The stacked data should be migrated to perform the seismic attribute analysis. These data might benefit from anisotropic rotation. We propose using the Harrison (1994) algorithm to do this. Migration has been attempted on some of the component sections, the resultant section shows an interesting anomaly near shot point 547 on P-P component section. The anomaly will need to be verified with more accurate velocity values. Because the geometry has not been properly completed, some difficulties are encountered when trying to store the migrated data on disk.

Prestacked data also are needed to apply *P-P* and *P-SV* AVO (Amplitude Versus Offset) analysis to further investigate the properties of lithology such as porosity or the permeability. Since we can think of a near offset stack as image P-wave impedance contrasts, while the far offset stack images Poisson's ratio contrasts. Different rotation methods will be tested to improve the quality of final sections.

ACKNOWLEDGMENT

We would like to thank Dr. Bee Bednar for donating the seismic data to CREWES project. We also thank Mssrs. Rick Walters, Dave Mackidd and Roger Banks, formerly of Amerada Hess Canada for helpful discussions.

REFERENCES

AHCL, 1993. Amerada Hess Corporation Limited internal file.

Domenico, S. N. , 1984, Rock lithology an porosity determination from shear and compressional wave velocity: Geophysics, 49, 1188 - 1195.

Ensley, R. A. , 1989, Analysis of compressional - and shear-wave seismic data from the Prudhoe Bay field: Geophysics The Leading Edge, 10 - 13.

Ensley, R. A. , 1985, Evaluation of direct hydrocarbon indicators through comparison of compressional and shear wave seismic dada: a case study of the Myrnam Gas Field, Alberta: Geophysics, 50, 37 - 48.

Ensley, R. A. , 1984, Comparison of P- and S- wave seismic data: a new method for detecting gas reservoirs: Geophysics, 49, 1420 - 1431.

Fertl, W. H. , 1978, Knowing basic reservoir parameters first step in log analysis: The Oil and Gas Journal, 98 - 118.

Garotta, R. , P. Marechal and M. Magesan, 1985, Two component acquisition as a routine procedure for recording P-waves and converted waves. J. of the Canadian Society of Exploration Geophysicists, V. 21, no. 1, 40 - 53.

Ikwuakor, K. C. , 1988, V_p / V_s revisited: pitfalls and new interpretation techniques, World Oil, September, 1988, 41 - 46.

Justice, M. G. , M. D. McCormack, and S. S. Lee, 1984, Anisotropy in the Morrow Formation of Southeast New Mexico : 54th. ann. International. mtg. Soc. Expl. Geoph. Expanded Abstract

McCormack, M. D. , J. A. Dunbar, and W.W. Sharp, 1984, A case study of stratigraphic interpretation using shear and compressional seismic data: Geophysics, 49, 509 - 520.

Omnes, G., 1978, Exploring with SH-waves: Can. Soc. Expl. Geophys. J., V. 14. 40-49.

Pardus, Y. C. , J. Conner, N. R. Schuler, and R.H. Tatham, 1990. V_p / V_s and lithology in Carbonate Rocks: A case study in the Scipio Trend in Southern Michigan. 60th. ann. International. mtg. Soc. Expl. Geoph. Expanded Abstract, 169 - 172.

Robertson, J. D. , 1987, Carbonate porosity from S / P traveltime ratios: Geophysics, 52, 1346 - 1354.

Robertson, J. D. , and W. C. Pritchett, 1985, Direct hydrocarbon detection using comparative P-wave and S-wave seismic sections: Geophysics, 50, 383 - 393.

Tatham, R. H. , 1982, V_p / V_s and lithology: Geophysics, 47, 336 - 344.

Tatham, R. H. , and P.L. Stoffa, 1976, V_p / V_s - A potential hydrocarbon indicator: Geophysics, 41, 895 - 921. Tatham, R. H. and M. D. McCormack, 1991, Multicomponent Seismology in Petroleum Exploration. Investigations in Geophysics Series Vol. 6. Society of Exploration Geophysics.

GEOMETRY	
Source type	vibroseis
Source interval	90 m
Group interval	15 m
Sweep frequency	8-80 Hz for *P* source, 8-50 Hz for *S* source
Sweep length	12
No. of sweeps	12
No. of traces / component	1520, (except *P-P* :1519, *SH-SV* :1516)
No. of channels / component	300
Total geophone spread	4575 m
Fold	50
RECORDING	
Recording system	I / O system two
Geophone type	OYO SMC
Sample rate	2 ms
Geophone frequency	10 Hz
Record length	6 sec
Notch filter	out
Low cut /High cut	3 Hz / 135 Hz

Table 2. Survey parameters for the nine-component 2-D line

P-P
2D Geometry
Minimum Phase Correction
Deconvolution
CDP Gather
Weathering Correction: refraction correction
Automatic Surface Consistent statics
Velocity Analysis
NMO
Surgical Band-pass Filter
Trace Muting
Automatic Trim Statics
CDP Stacking
Zero-phase Band-pass Filtering : 10/15 - 70/80 Hz
Scaling: multiple gate balance
Display : 7.5 in / sec
P-S
2D Geometry
Minimum Phase Correction
Velocity Specific Filtering: rejected velocity 900-2100 m/sec
Deconvolution
CDP Gather
Weathering Correction: shot statics
Velocity Analysis
Residual Statics
Automatic Surface Consistent statics
Velocity Analysis
NMO
Trace Muting
Calculate V_p/V_s ratio (from travel times on *P* and *P-S*)
Automatic Trim Statics
CCP Stacking
Zero-phase Band-pass Filtering : 8/12 - 35/45 Hz
Scaling: AGC (500 ms window)
Display: 5 in / sec

Table 3. Processing flow of *P* and *P-S* data

S-S
2D Geometry
Minimum Phase Correction
Velocity Specific Filtering: rejected velocity
650 - 1850 m/sec for pure *S*
750 - 1600 m/sec for *SV-SH, SH-SV*
Deconvolution
CDP Gather
Weathering Correction: refraction correction for pure *S*
shot and receiver statics for *SV-SH, SH-SV*
Automatic Surface Consistent statics
Velocity Analysis
NMO
Weighted Trace Mix for *SH-SV* and *SV-SH*
Trace Muting
Automatic Trim Statics for pure *S*
CDP Stacking
Zero-phase Band-pass Filtering : 5/8 - 30/35 Hz
Scaling: AGC (500 ms window)
Display: 3.75 in / sec
S-P
2D Geometry
Minimum Phase Correction
Deconvolution
CDP Gather
Weathering Correction: shot and receiver statics
Automatic Surface Consistent statics: final shot and receiver statics
Velocity Analysis
NMO
Trace Muting
Depth Variant Mapping using $V_p/V_s = 2$
CCP Stacking
Zero-phase Band-pass Filtering : 8/12 - 35/45 Hz
Scaling: AGC (500 ms window)
Display: 5 in / sec

Table 4 Processing flow of S and S-converted wave data

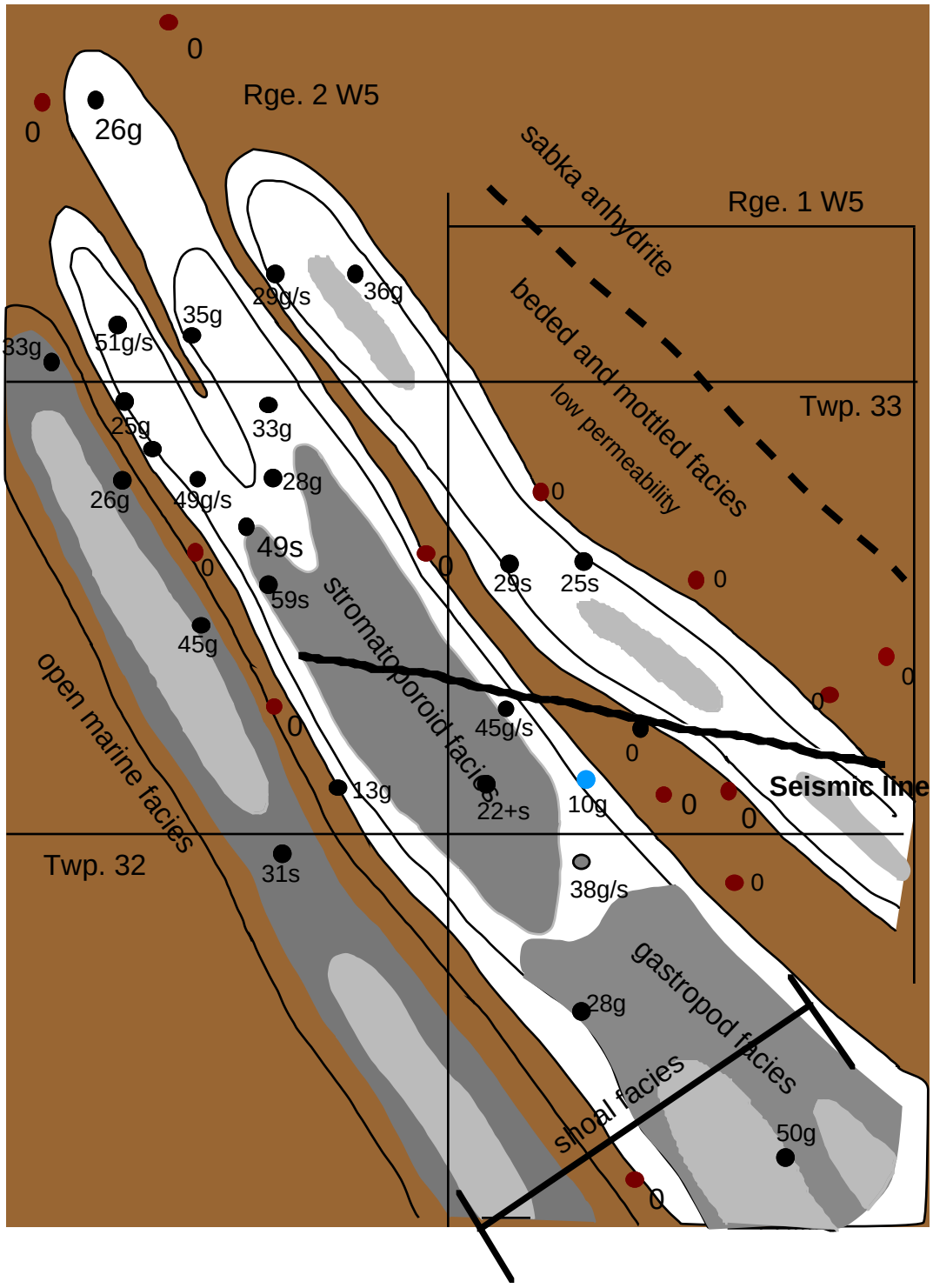

Fig. 3 Geological model base on the core analysis. Darker area are beded and mottled facies, stromatoporoid and gastropod facies are shaded in ligher tone.

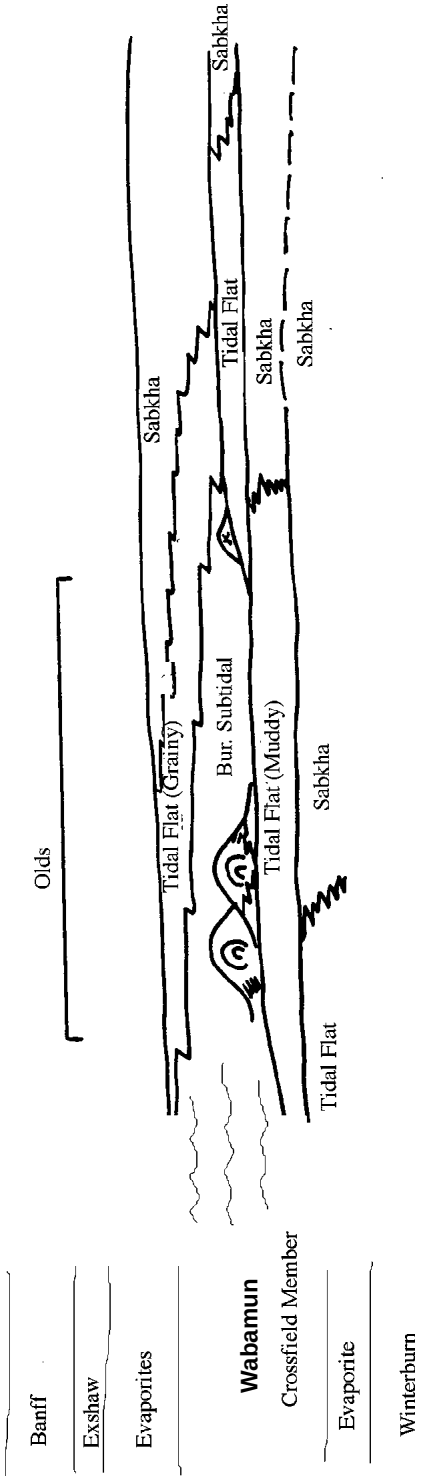

Fig. 4. Stratigraphic nomenclature and distribution of facies for the upper Devonian in Olds, Alberta

P-P

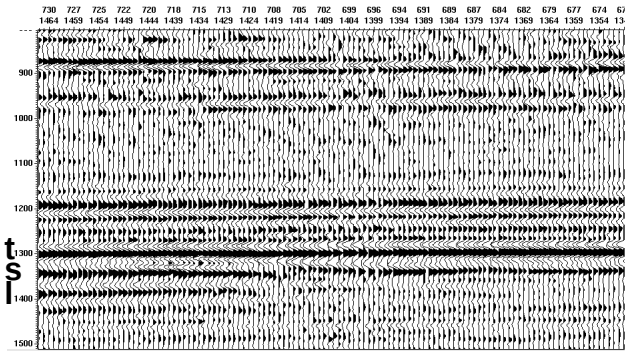

Fig. 5a *P-P* component

P-SV

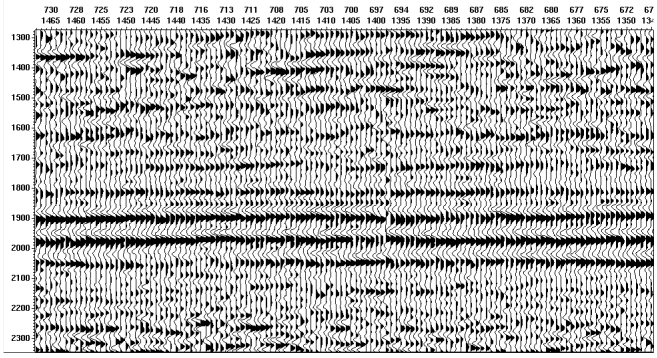

Fig. 5b *P-SV* component

P-SH

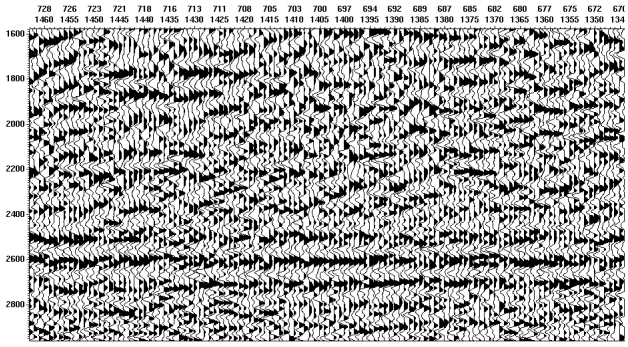

Fig. 5c *P-SH* component

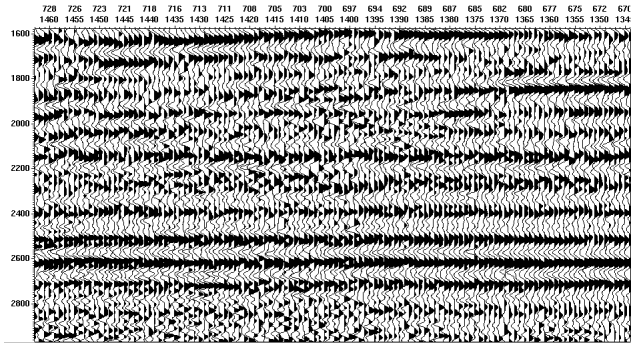

Fig. 5d *SV-SV* component

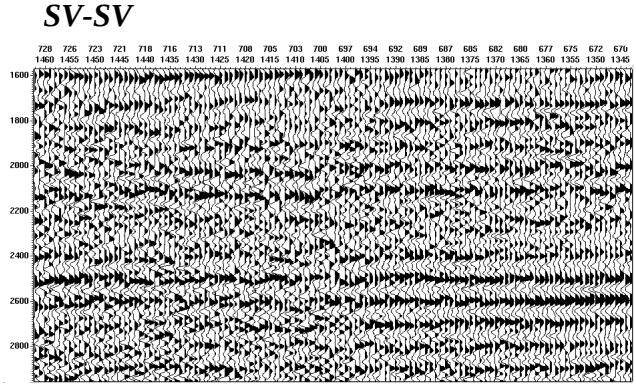

Fig. 5e *SH-SH* component

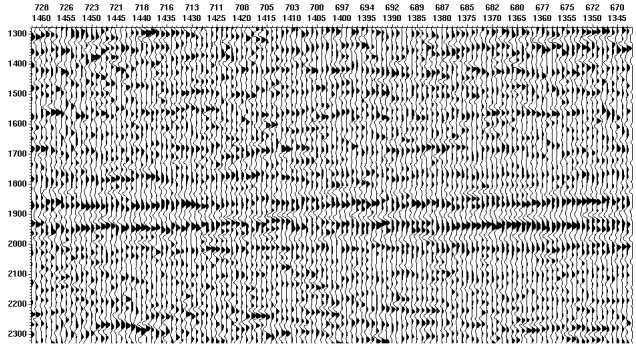

Fig. 5f *SV-P* component

SH-P

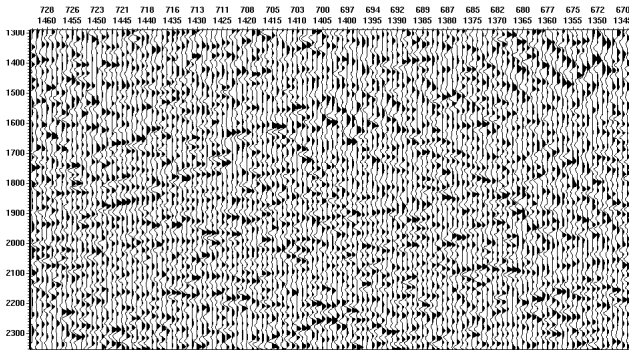

Fig. 5g *SH-P* component

SV-SH

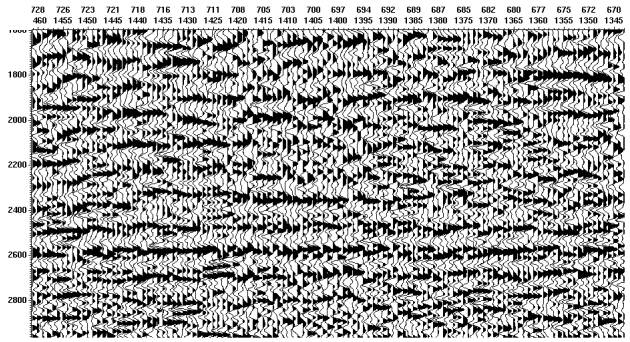

Fig. 5h *SV-SH* component

SH-SV

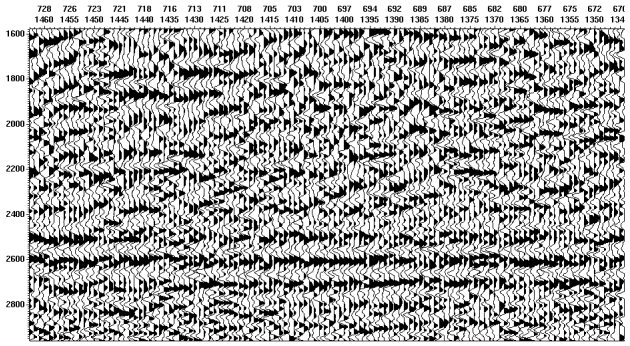

Fig. 5i *SH-SV* component

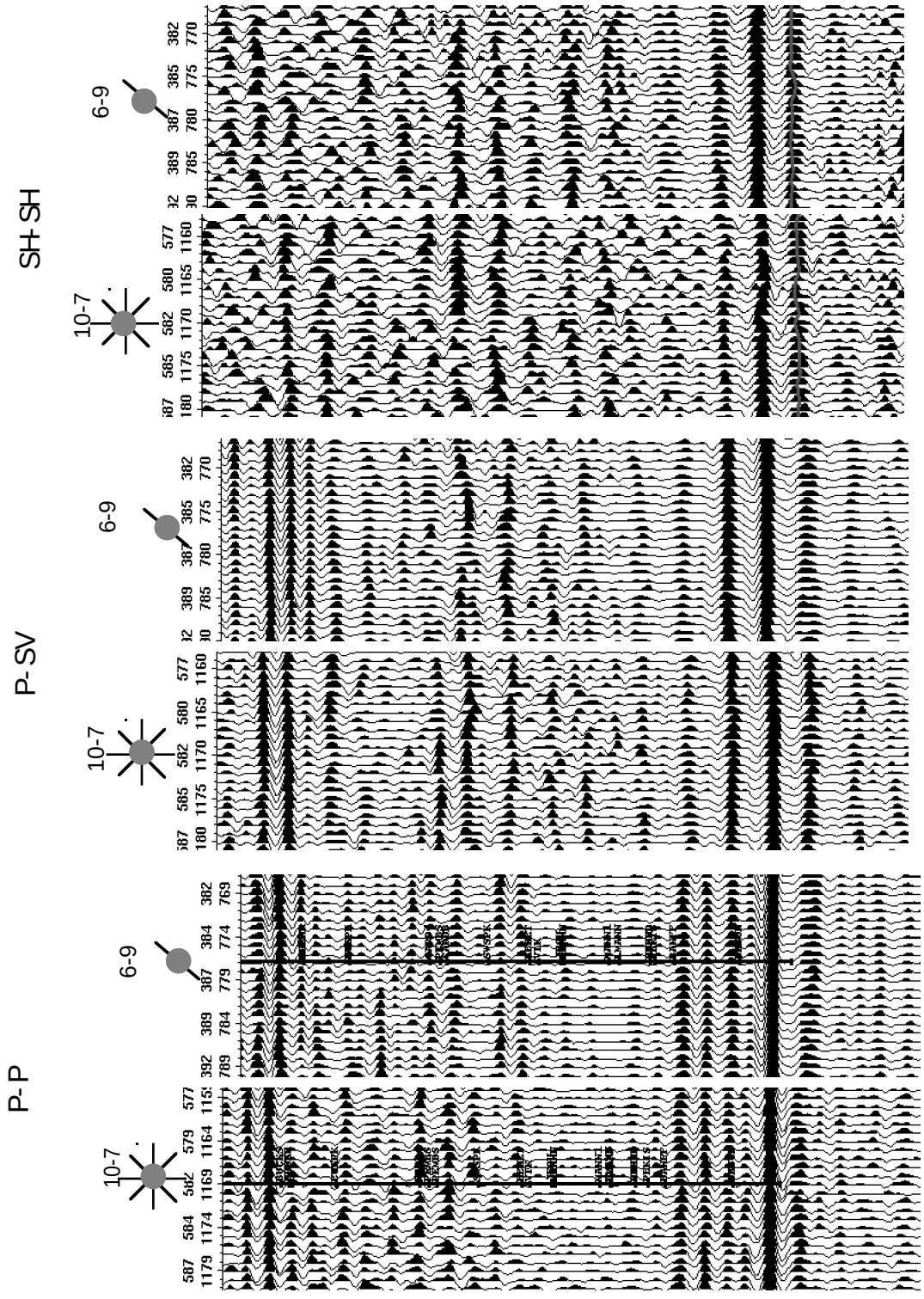

Fig. 6. Seismic line of *P-P* , *P-SV*, and *SH-SH* near the wells

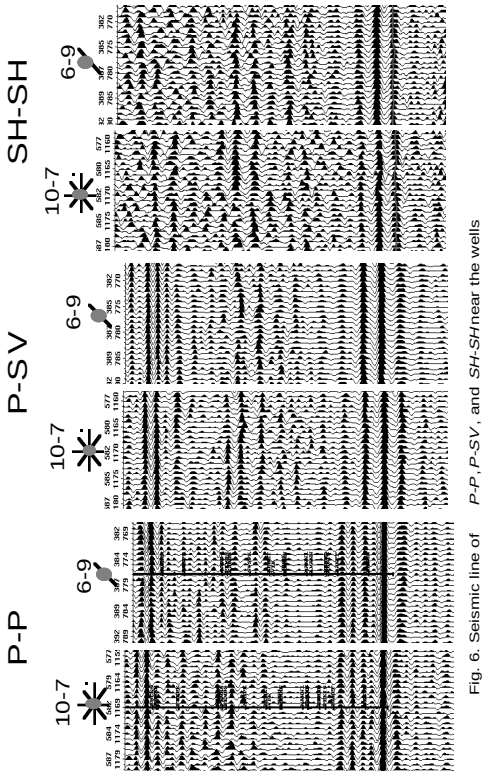

Fig. 6. Seismic line of *P-P*, *P-SV*, and *SH-SH* near the wells

Fig. 7. Correlation between *P-P*, *P-SV*, and *SH-SH* sections

Fig. 8. V_p/V_s versus shot point

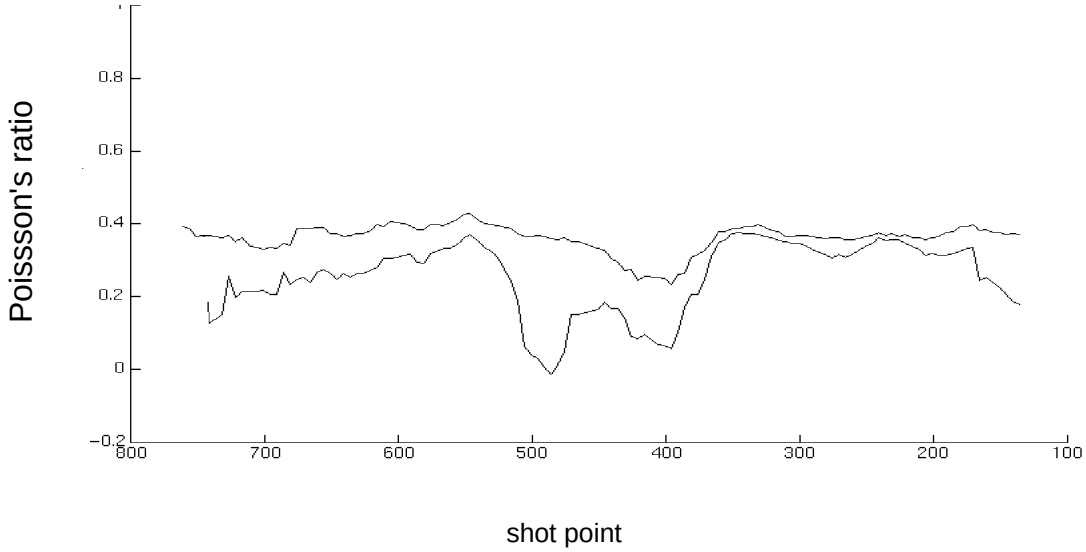

Fig. 9. Poisson's ratio versus shot point

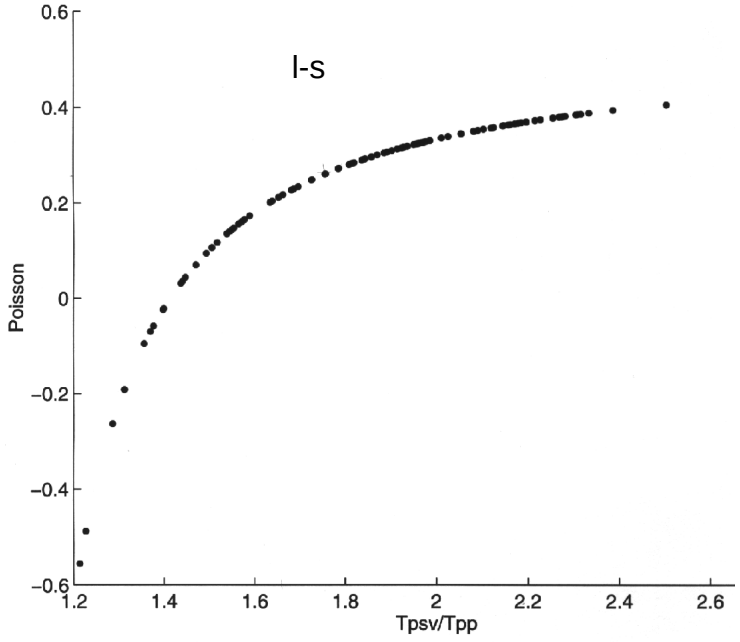

Fig. 10. Poisson's ration versus traveltime ratio (T_{psv}/T_{pp})

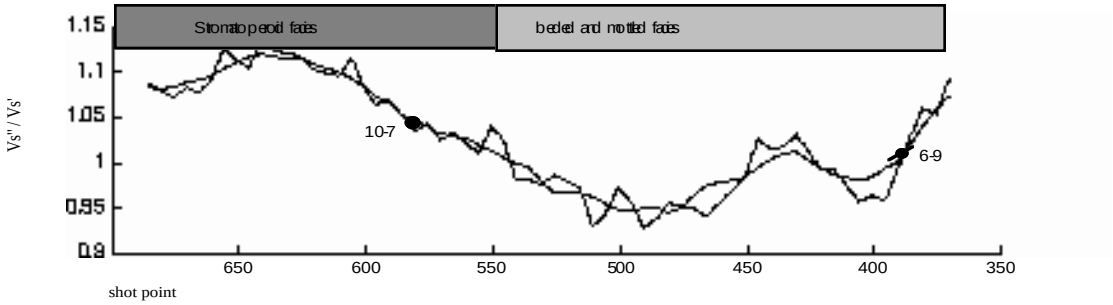

Fig. 11. V_{SH}/ V_{SV} versus shot point